

# Experimental implementation of tightly focused beams with unpolarized transversal component at any plane

Rosario Martínez-Herrero,<sup>1</sup> David Maluenda,<sup>2</sup> Ignasi Juvells,<sup>2</sup> and Artur Carnicer<sup>2,\*</sup>

<sup>1</sup>*Departamento de Óptica, Facultad de Ciencias Físicas, Universidad Complutense de Madrid, 28040 Madrid, Spain*

<sup>2</sup>*Departament de Física Aplicada i Òptica, Universitat de Barcelona (UB), Martí i Franquès 1, 08028 Barcelona, Spain*

\*[artur.carnicer@ub.edu](mailto:artur.carnicer@ub.edu)

**Abstract:** The aim of this paper is to provide a formal framework for designing highly focused fields with specific transversal features when the incoming beam is partially polarized. More specifically, we develop a field with a transversal component that remains unpolarized in the focal area. Special attention is paid to the design of the input beam and the development of the experiment. The implementation of such fields is possible by using an interferometric setup combined with the use of digital holography techniques. Experimental results are compared with those obtained numerically.

© 2014 Optical Society of America

**OCIS codes:** (260.5430) Polarization; (090.1760) Computer holography; (070.6120) Spatial light modulators.

---

## References

1. R. Dorn, S. Quabis, and G. Leuchs, "Sharper focus for a radially polarized light beam," *Phys. Rev. Lett.* **91**, 233901 (2003).
2. N. Davidson and N. Bokor, "High-numerical-aperture focusing of radially polarized doughnut beams with a parabolic mirror and a flat diffractive lens," *Opt. Lett.* **29**, 1318–1320 (2004).
3. M. Leutenegger, R. Rao, R. A. Leitgeb, and T. Lasser, "Fast focus field calculations," *Opt. Express* **14**, 11277–11291 (2006).
4. Y. Kozawa and S. Sato, "Sharper focal spot formed by higher-order radially polarized laser beams," *J. Opt. Soc. Am. A* **24**, 1793–1798 (2007).
5. H. Wang, L. Shi, B. Lukyanchuk, C. Sheppard, and C. T. Chong, "Creation of a needle of longitudinally polarized light in vacuum using binary optics," *Nat. Photonics* **2**, 501–505 (2008).
6. G. M. Lerman and U. Levy, "Effect of radial polarization and apodization on spot size under tight focusing conditions," *Opt. Express* **16**, 4567–4581 (2008).
7. X. Hao, C. Kuang, T. Wang, and X. Liu, "Phase encoding for sharper focus of the azimuthally polarized beam," *Opt. Lett.* **35**, 3928–3930 (2010).
8. S. N. Khonina and S. G. Volotovskiy, "Controlling the contribution of the electric field components to the focus of a high-aperture lens using binary phase structures," *J. Opt. Soc. Am. A* **27**, 2188–2197 (2010).
9. M. R. Foreman, S. S. Sherif, P. R. Munro, and P. Török, "Inversion of the debye-wolf diffraction integral using an eigenfunction representation of the electric fields in the focal region," *Opt. Express* **16**, 4901–4917 (2008).
10. K. Jahn and N. Bokor, "Solving the inverse problem of high numerical aperture focusing using vector spheroidal harmonics and vector spheroidal multipole fields," *Opt. Commun.* **288**, 13–16 (2013).
11. C. Maurer, A. Jesacher, S. Fürhapter, S. Bernet, and M. Ritsch-Marte, "Tailoring of arbitrary optical vector beams," *New J. Phys.* **9**, 78 (2007).
12. X.L. Wang, J. Ding, W.J. Ni, C.S. Guo, and H.T. Wang, "Generation of arbitrary vector beams with a spatial light modulator and a common path interferometric arrangement," *Opt. Lett.* **32**, 3549–3551 (2007).
13. H.T. Wang, X.L. Wang, Y. Li, J. Chen, C.S. Guo, and J. Ding, "A new type of vector fields with hybrid states of polarization," *Opt. Express* **18**, 10786–10795 (2010).

14. I. Moreno, C. Iemmi, J. Campos, and M. J. Yzuel, "Jones matrix treatment for optical fourier processors with structured polarization," *Opt. Express* **19**, 4583–4594 (2011).
15. F. Kenny, D. Lara, O. Rodríguez-Herrera, and C. Dainty, "Complete polarization and phase control for focus-shaping in high-NA microscopy," *Opt. Express* **20**, 14015–14029 (2012).
16. R. Martínez-Herrero, I. Juvells, and A. Carnicer, "On the physical realizability of highly focused electromagnetic field distributions," *Opt. Lett.* **38**, 2065–2067 (2013).
17. D. Maluenda, I. Juvells, R. Martínez-Herrero, and A. Carnicer, "Reconfigurable beams with arbitrary polarization and shape distributions at a given plane," *Opt. Express* **21**, 5432–5439 (2013).
18. D. Maluenda, R. Martínez-Herrero, I. Juvells, and A. Carnicer, "Synthesis of highly focused fields with circular polarization at any transverse plane," *Opt. Express* **22**, 6859–6867 (2014).
19. G. Brakenhoff, P. Blom, and P. Barends, "Confocal scanning light microscopy with high aperture immersion lenses," *J. Microsc.* **117**, 219–232 (1979).
20. C. J. Sheppard and A. Choudhury, "Annular pupils, radial polarization, and superresolution," *Appl. Opt.* **43**, 4322–4327 (2004).
21. K. Kitamura, K. Sakai, and S. Noda, "Sub-wavelength focal spot with long depth of focus generated by radially polarized, narrow-width annular beam," *Opt. Express* **18**, 4518–4525 (2010).
22. W. Wang, A. T. Friberg, and E. Wolf, "Focusing of partially coherent light in systems of large Fresnel numbers," *J. Opt. Soc. Am. A* **14**, 491–496 (1997).
23. K. Lindfors, T. Setälä, M. Kaivola, and A. T. Friberg, "Degree of polarization in tightly focused optical fields," *J. Opt. Soc. Am. A* **22**, 561–568 (2005).
24. K. Lindfors, A. Priimagi, T. Setälä, A. Shevchenko, A. T. Friberg, and M. Kaivola, "Local polarization of tightly focused unpolarized light," *Nat. Photonics* **1**, 228–231 (2007).
25. M. R. Foreman and P. Török, "Focusing of spatially inhomogeneous partially coherent, partially polarized electromagnetic fields," *J. Opt. Soc. Am. A* **26**, 2470–2479 (2009).
26. L.-P. Leppänen, A. T. Friberg, and T. Setälä, "Partial polarization of optical beams and near fields probed with a nanoscatterer," *J. Opt. Soc. Am. A* **31**, 1627–1635 (2014).
27. J. M. Auñón and M. Nieto-Vesperinas, "Partially coherent fluctuating sources that produce the same optical force as a laser beam," *Opt. Lett.* **38**, 2869–2872 (2013).
28. J. M. Auñón and M. Nieto-Vesperinas, "On two definitions of the three-dimensional degree of polarization in the near field of statistically homogeneous partially coherent sources," *Opt. Lett.* **38**, 58–60 (2013).
29. K. H. Kim, B. H. Park, Y. Tu, T. Hasan, B. Lee, J. Li, and J. F. de Boer, "Polarization-sensitive optical frequency domain imaging based on unpolarized light," *Opt. Express* **19**, 552–561 (2011).
30. J. A. Fan, K. Bao, J. B. Lassiter, J. Bao, N. J. Halas, P. Nordlander, and F. Capasso, "Near-normal incidence dark-field microscopy: applications to nanoplasmonic spectroscopy," *Nano Lett.* **12**, 2817–2821 (2012).
31. T. Ergin, N. Stenger, P. Brenner, J. B. Pendry, and M. Wegener, "Three-dimensional invisibility cloak at optical wavelengths," *Science* **328**, 337–339 (2010).
32. R. Martínez-Herrero, I. Juvells, and A. Carnicer, "Design of highly focused fields that remain unpolarized on axis," *Opt. Lett.* **39** (2014).
33. B. Richards and E. Wolf, "Electromagnetic diffraction in optical systems. ii. structure of the image field in an aplanatic system," *Proc. R. Soc. London, Ser. A* **253**, 358–379 (1959).
34. Q. Zhan, "Properties of circularly polarized vortex beams," *Opt. Lett.* **31**, 867–869 (2006).
35. R. Martínez-Herrero and P. Mejías, "Angular momentum decomposition of nonparaxial light beams," *Opt. Express* **18**, 7965–7971 (2010).
36. A. Y. Bekshaev, "A simple analytical model of the angular momentum transformation in strongly focused light beams," *Cent. Eur. J. Phys.* **8**, 947–960 (2010).
37. M. Born and E. Wolf, *Principles of Optics: Electromagnetic Theory of Propagation, Interference and Diffraction of Light* (Cambridge University, 1999).
38. V. Arrizón, "Complex modulation with a twisted-nematic liquid-crystal spatial light modulator: double-pixel approach," *Opt. Lett.* **28**, 1359–1361 (2003).

## 1. Introduction

Three dimensional electromagnetic field distributions generated at the focal region of a high numerical aperture (NA) focused system has been extensively investigated in the last years [1–21]. Non-paraxial fields have demonstrated very useful in many fields for instance in high-resolution microscopy, particle trapping, high-density recording, tomography, electron acceleration, non-linear optics, and optical tweezers. In most of the cases the study is concentrated on fully polarized fields. However, partially polarized tightly focused fields are attracting some more attention [22–28]. Tailoring three dimensional vectorial electromagnetic distributions with specified characteristics (shape, polarization, coherence, angular moment, etcetera) requires a careful de-

sign of the incident beam. The objective of this paper is to develop a method for designing focused fields with a non-polarized transversal component at any plane in the focal area and a non-zero longitudinal component on axis. This kind of fields may be useful in tomography, plasmonics spectroscopy, or invisibility cloaking [29–31].

Very recently we developed a framework for analyzing focused fields with specific polarization features when the optical system is illuminated with partially polarized light. This method relates the circular content of the incident beam with the circular and longitudinal components of the focused field [32]. Using this formalism, in this paper we derive analytical expressions that link the coherence-polarization properties of a quasi-monochromatic statistically stationary incident beam and the transversal part of a focused field. Taking these equations into account, we provide sufficient conditions for the incident beam so as to obtain fields in the focal area whose transversal component remains unpolarized for any  $z$ . These class of beams are implemented experimentally by means of spatial light modulators (SLM) displaying computer generated holograms. Numerical calculations and experimental results are compared and analysed.

Accordingly, the paper is organized as follows: in section 2 we review the description of highly focused partially polarized beams in terms of the angular spectrum. In section 3, this framework is used for designing focused fields whose transversal part remains unpolarized for any  $z$ . Section 4 includes an explanation of the optical setup used for generating these kind of beams. Experimental results are presented and discussed. Finally, the main conclusions of this paper are summarized in section 5.

## 2. Review of basic concepts

The electric field distribution at any point in the focal region of a high numerical aperture focusing system is given by the well know Richards-Wolf integral [33]

$$\mathbf{E}(r, \varphi, z) = A \int_0^{\theta_0} \int_0^{2\pi} P(\theta) \mathbf{E}_0(\theta, \phi) e^{ik \sin \theta r \cos(\varphi - \phi)} e^{-ik \cos \theta z} \sin \theta d\theta d\phi, \quad (1)$$

where  $A$  is a constant, related to the focal length and the wavelength,  $k$  is the wave number,  $r$  and  $\varphi$  denote here the polar coordinates at the focal plane, and angles  $\phi$ ,  $\theta$  and  $\theta_0$  are represented in Fig. 1.  $P(\theta)$  denotes the so called apodization function obtained from energy conservation and geometric considerations. According to the characteristics of the problem, it can be advisable to write the angular spectrum  $\mathbf{E}_0$  in terms of the circular content of the beam instead of using the conventional radial and azimuthal description [34]:

$$\mathbf{E}_0(\theta, \phi) = g_1(\theta, \phi) \mathbf{v}_1(\theta, \phi) + g_2(\theta, \phi) \mathbf{v}_2(\theta, \phi), \quad (2)$$

where  $g_1$  and  $g_2$  are, respectively, the right-hand and left-hand circular components of the incident field and  $\mathbf{v}_1$  and  $\mathbf{v}_2$  are mutually orthogonal unitary vectors that can be described in terms of the radial and azimuthal vectors  $\mathbf{e}_1$  and  $\mathbf{e}_2$  by means of

$$\mathbf{v}_1(\theta, \phi) = \frac{e^{i\phi}}{\sqrt{2}} (\mathbf{e}_2 + i\mathbf{e}_1) \quad (3a)$$

$$\mathbf{v}_2(\theta, \phi) = \frac{e^{-i\phi}}{\sqrt{2}} (\mathbf{e}_2 - i\mathbf{e}_1), \quad (3b)$$

where

$$\mathbf{e}_1(\phi) = (-\sin \phi, \cos \phi, 0) \quad (4a)$$

$$\mathbf{e}_2(\theta, \phi) = (\cos \theta \cos \phi, \cos \theta \sin \phi, \sin \theta). \quad (4b)$$

$\mathbf{v}_m(\theta, \phi) \exp(ik\mathbf{r} \cdot \mathbf{s})$  ( $m = 1, 2$ ) are circularly polarized planar waves propagating along the direction defined by  $\mathbf{s} = (\sin \theta \cos \phi, \sin \theta \sin \phi, -\cos \theta)$ . Angular spectrum  $\mathbf{E}_0$  can be understood as the superposition of right and left circularly polarized plane waves. Notice that in the paraxial limit ( $\theta \rightarrow 0$ ),  $\mathbf{v}_1 = \frac{1}{\sqrt{2}}(1, i, 0)$  and  $\mathbf{v}_2 = \frac{1}{\sqrt{2}}(1, -i, 0)$  are the usual transversal circular plane waves.

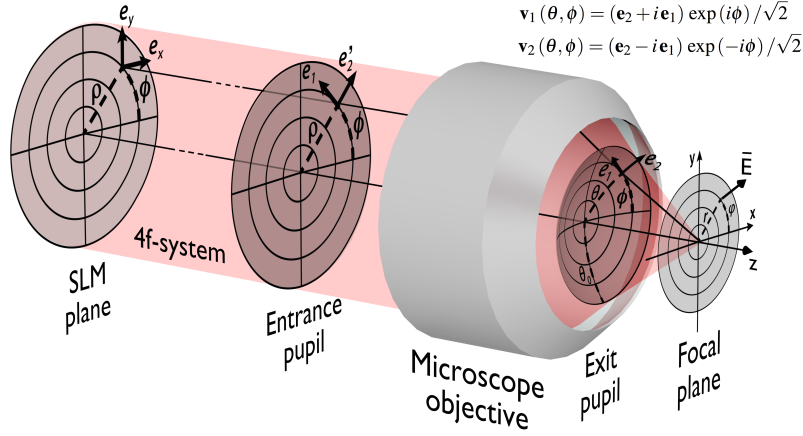


Fig. 1. Geometry, bases and variables involved.

The use of this circular basis is particularly useful in the analysis of the angular momentum and when dealing with vortex beams [34–36]. Moreover, this basis is very suitable for designing the polarization characteristics of the transverse component of a highly focused beam [18, 32]. We rewrite the field at the vicinity of the focus plane  $\mathbf{E}$  as follows:

$$\mathbf{E} = \mathbf{E}_c \begin{pmatrix} \frac{1}{\sqrt{2}} & \frac{i}{\sqrt{2}} & 0 \\ 1 & -i & 0 \\ \frac{\sqrt{2}}{0} & \frac{\sqrt{2}}{0} & 1 \end{pmatrix}. \quad (5)$$

where  $\mathbf{E}_c = (E_+, E_-, E_z)$ ; here  $E_+$  and  $E_-$  represent the right and left circular content of the transverse field at the vicinity of the focus plane, and  $E_z$  is the magnitude of the longitudinal component. Taking into account Eqs. (2) and (5), Eq. (1) is rewritten as

$$\mathbf{E}_c(r, \varphi, z) = A \int_0^{\theta_0} \int_0^{2\pi} \mathbf{g}(\theta, \phi) \hat{A}(\theta, \phi) P(\theta) e^{ik \sin \theta r \cos(\phi - \varphi)} e^{-ik \cos \theta z} \sin \theta d\theta d\phi, \quad (6)$$

where  $\mathbf{g} = (g_1, g_2)$  and  $\hat{A}(\theta, \phi)$  is a 2x3 matrix given by

$$\hat{A}(\theta, \phi) = \begin{pmatrix} \cos^2(\theta/2) & -\sin^2(\theta/2)e^{2i\phi} & \frac{1}{\sqrt{2}} \sin \theta e^{i\phi} \\ -\sin^2(\theta/2)e^{-2i\phi} & \cos^2(\theta/2) & \frac{1}{\sqrt{2}} \sin \theta e^{-i\phi} \end{pmatrix}. \quad (7)$$

Thus, Eq. (6) relates the circular components of incident field with the circular and longitudinal content of focused field.

Let us next consider a quasi-monochromatic statistically stationary incident beam. On the one hand, the coherence-polarization features of the input paraxial beam are characterized by means

of the 2x2 matrix  $\widehat{G}$  defined as

$$\widehat{G}(\theta_1, \phi_1, \theta_2, \phi_2) = \langle \mathbf{g}^\dagger(\theta_1, \phi_1) \mathbf{g}(\theta_2, \phi_2) \rangle, \quad (8)$$

where the dagger  $\dagger$  stands for transpose complex conjugate and the angular brackets indicate statistical average. On the other hand, the coherence-polarization properties of the focused field are fully contained in the 3x3 cross-spectral density matrix  $\widehat{W}_c$  given by

$$\widehat{W}_c(r_1, \varphi_1, r_2, \varphi_2, z) = \langle \mathbf{E}_c^\dagger(r_1, \varphi_1, z) \mathbf{E}_c(r_2, \varphi_2, z) \rangle. \quad (9)$$

By using Eqs. (6), (8) and (9) the relationship between  $\widehat{W}_c$  and  $\widehat{G}$  is obtained:

$$\begin{aligned} \widehat{W}_c(r_1, \varphi_1, r_2, \varphi_2, z) &= |A|^2 \int_0^{\theta_0} \int_0^{\theta_0} \int_0^{2\pi} \int_0^{2\pi} \widehat{A}(\theta_1, \phi_1)^\dagger \widehat{G}(\theta_1, \phi_1, \theta_2, \phi_2) \widehat{A}(\theta_2, \phi_2) \\ &\quad P(\theta_1) P(\theta_2) \exp(-ik\mathbf{r}_1 \cdot \mathbf{s}_1) \exp(ik\mathbf{r}_2 \cdot \mathbf{s}_2) \sin \theta_1 \sin \theta_2 d\theta_1 d\theta_2 d\phi_1 d\phi_2. \end{aligned} \quad (10)$$

where  $\mathbf{r}_j = (r_j \cos \phi_j, r_j \sin \phi_j, z)$  and  $\mathbf{s}_j = (\sin \theta_j \cos \varphi_j, \sin \theta_j \sin \varphi_j, -\cos \theta_j)$  with  $j = 1, 2$ . Eq. (10) relates coherence-polarization properties of the incident and the focused field in terms of the circular polarization content.

### 3. Focused fields with unpolarized transversal component

In this section we concentrate on the transverse field components of Eq. (10):

$$\begin{aligned} \widehat{W}_{cT}(r_1, \varphi_1, r_2, \varphi_2, z) &= |A|^2 \int_0^{\theta_0} \int_0^{\theta_0} \int_0^{2\pi} \int_0^{2\pi} \widehat{A}_T(\theta_1, \phi_1)^\dagger \widehat{G}(\theta_1, \phi_1, \theta_2, \phi_2) \widehat{A}_T(\theta_2, \phi_2) \\ &\quad P(\theta_1) P(\theta_2) \exp(-ik\mathbf{r}_1 \cdot \mathbf{s}_1) \exp(ik\mathbf{r}_2 \cdot \mathbf{s}_2) \sin \theta_1 \sin \theta_2 d\theta_1 d\theta_2 d\phi_1 d\phi_2. \end{aligned} \quad (11)$$

where  $\widehat{W}_{cT}$  is a 2x2 matrix containing the transverse part of  $\widehat{W}_c$ , and  $\widehat{A}_T$  is the 2x2 matrix defined as

$$\widehat{A}_T(\theta, \phi) = \begin{pmatrix} \cos^2(\theta/2) & -\sin^2(\theta/2)e^{2i\phi} \\ -\sin^2(\theta/2)e^{-2i\phi} & \cos^2(\theta/2) \end{pmatrix}. \quad (12)$$

Let us now introduce  $\widehat{G}_T$  defined as

$$\widehat{G}_T(\theta_1, \phi_1, \theta_2, \phi_2) = \widehat{A}_T(\theta_1, \phi_1)^\dagger \widehat{G}(\theta_1, \phi_1, \theta_2, \phi_2) \widehat{A}_T(\theta_2, \phi_2) \quad (13)$$

thus Eq. (11) can now be written in a more compact way

$$\begin{aligned} \widehat{W}_{cT}(r_1, \varphi_1, r_2, \varphi_2, z) &= |A|^2 \int_0^{\theta_0} \int_0^{\theta_0} \int_0^{2\pi} \int_0^{2\pi} \widehat{G}_T(\theta_1, \phi_1, \theta_2, \phi_2) P(\theta_1) P(\theta_2) \\ &\quad \exp(-ik\mathbf{r}_1 \cdot \mathbf{s}_1) \exp(ik\mathbf{r}_2 \cdot \mathbf{s}_2) \sin \theta_1 \sin \theta_2 d\theta_1 d\theta_2 d\phi_1 d\phi_2. \end{aligned} \quad (14)$$

To analyse the polarization of the transversal component we write the matrix  $\widehat{W}_{cT}(r, \varphi, r, \varphi, z)$ , namely  $\widehat{W}_{cT}(r, \varphi, z)$ , in terms of the circular Stokes parameters  $C_n(r, z) = \text{tr}(\widehat{W}_{cT}(r, \varphi, z) \sigma_n)$  with  $n = 0, 1, 2, 3$ ;  $\sigma_n$  are the Pauli matrices [37]. According to Eq. (14),

$$\begin{aligned} C_n(r, z) &= |A|^2 \int_0^{\theta_0} \int_0^{\theta_0} \int_0^{2\pi} \int_0^{2\pi} C_{nT}(\theta_1, \phi_1, \theta_2, \phi_2) P(\theta_1) P(\theta_2) \\ &\quad \exp(-ik\mathbf{r}_1 \cdot \mathbf{s}_1) \exp(ik\mathbf{r}_2 \cdot \mathbf{s}_2) \sin \theta_1 \sin \theta_2 d\theta_1 d\theta_2 d\phi_1 d\phi_2 \end{aligned} \quad (15)$$

being  $C_{nT}$

$$C_{nT}(\theta_1, \phi_1, \theta_2, \phi_2) = \text{tr} \left( \widehat{G}_T(\theta_1, \phi_1, \theta_2, \phi_2) \sigma_n \right). \quad (16)$$

$C_{nT}$  are the so-called circular generalized Stokes parameters as they are the analogue of the generalized Stokes parameters [37]. Eq. (15) is one of the main results of this paper, since provides the relationship between the polarization properties of the incident beam and the transversal part of focused field, in terms of the circular Stokes parameters.

An interesting application of the formalism developed above is the design of a field in the focal area whose transversal part is non-polarized. Taken Eq. (15) into account, the transversal field is unpolarized when  $C_n(r, z) = 0$  for  $n = 1, 2, 3$ . To this end we consider a beam whose circular generalized Stokes parameters are given by

$$C_{0T}(\theta_1, \phi_1, \theta_2, \phi_2) = 4h(\theta_1, \theta_2) \cos(m(\phi_1 - \phi_2)) \quad (17a)$$

$$C_{1T}(\theta_1, \phi_1, \theta_2, \phi_2) = 4ih(\theta_1, \theta_2) \sin(m(\phi_1 - \phi_2)) \quad (17b)$$

$$C_{2T}(\theta_1, \phi_1, \theta_2, \phi_2) = C_{3T}(\theta_1, \phi_1, \theta_2, \phi_2) = 0 \quad (17c)$$

here  $h(\theta_1, \theta_2)$  is a nonnegative definite function fulfilling  $h(\theta_1, \theta_2) = h(\theta_2, \theta_1)^*$ . These Stokes parameters correspond to a matrix  $\widehat{G}_T$  given by

$$\widehat{G}_T(\theta_1, \phi_1, \theta_2, \phi_2) = h(\theta_1, \theta_2) \widehat{U}^\dagger(\phi_1) \widehat{U}(\phi_2) \quad (18)$$

where

$$\widehat{U}(\phi) = \begin{pmatrix} -ie^{-im\phi} & ie^{im\phi} \\ e^{-im\phi} & e^{im\phi} \end{pmatrix}. \quad (19)$$

Substituting Eq. (17) into (15) we get

$$C_0(r, z) = 16\pi^2 |A|^2 \int_0^{\theta_0} \int_0^{\theta_0} P(\theta_1) P(\theta_2) h(\theta_1, \theta_2) J_m(kr \sin \theta_1) J_m(kr \sin \theta_2) \exp(-ikrz \cos \theta_2) \exp(ikz \cos \theta_1) \sin \theta_1 \sin \theta_2 d\theta_1 d\theta_2 \quad (20a)$$

$$C_1(r, z) = C_2(r, z) = C_3(r, z) = 0 \quad (20b)$$

Hence, a field whose transversal part is unpolarized for any  $z$  and vanishes on axis is obtained, regardless of the form of function  $h$ . According to Eqs. (13) and (18), the matrix of incident beam  $\widehat{G}$  now reads

$$\widehat{G}(\theta_1, \phi_1, \theta_2, \phi_2) = h(\theta_1, \theta_2) \left( \widehat{A}_T(\theta_2, \phi_2)^\dagger \right)^{-1} \widehat{U}^\dagger(\phi_1) \widehat{U}(\phi_2) \widehat{A}_T(\theta_2, \phi_2)^{-1}. \quad (21)$$

Using Eqs. (10) and (21), and after some calculations, the following expression for the longitudinal component of the focused field is obtained:

$$\widehat{W}_c(r_1, \phi_1, r_2, \phi_2, z)_{zz} = 8\pi^2 |A|^2 \cos((m-1)(\phi_1 - \phi_2)) \int_0^{\theta_0} \int_0^{\theta_0} P(\theta_1) P(\theta_2) h(\theta_1, \theta_2) \tan \theta_1 \tan \theta_2 \exp(-ikrz \cos \theta_2) \exp(ikz \cos \theta_1) J_{m-1}(kr_1 \sin \theta_1) J_{m-1}(kr_2 \sin \theta_2) \sin \theta_1 \sin \theta_2 d\theta_1 d\theta_2 \quad (22)$$

From Eq. (22) we conclude that, on axis, the irradiance of the longitudinal component vanishes when  $m \neq 1$ . However, for  $m = 1$  the field is purely longitudinal on axis, and its irradiance becomes

$$I(0, z) = \text{tr}(\widehat{W}_c(0, \varphi, 0, \varphi, z)) = 8\pi^2 |A|^2 \int_0^{\theta_0} \int_0^{\theta_0} P(\theta_1) P(\theta_2) h(\theta_1, \theta_2) \tan \theta_1 \tan \theta_2 \exp(-ikrz \cos \theta_2) \exp(ikz \cos \theta_1) \sin \theta_1 \sin \theta_2 d\theta_1 d\theta_2 \quad (23)$$

Since fields with longitudinal component are relevant in several applications, from this point onwards, we analyse the case  $m = 1$  thus Eq. (21) becomes

$$\widehat{G}(\theta_1, \phi_1, \theta_2, \phi_2) = h(\theta_1, \theta_2) \begin{pmatrix} ae^{i(\phi_1 - \phi_2)} & be^{i(\phi_1 + \phi_2)} \\ be^{-i(\phi_1 + \phi_2)} & ae^{-i(\phi_1 - \phi_2)} \end{pmatrix} \quad (24)$$

with

$$\begin{aligned} a &= 1 + \cos \theta_1 \cos \theta_2 \\ b &= 1 - \cos \theta_1 \cos \theta_2 \end{aligned} \quad (25)$$

A calculation of the beam proposed in Eq. (24) has been carried out using Eq. (10) and assuming a constant value for function  $h$ . The results are presented in Fig. 2. The first row shows the intensity of the focused field at  $z = 0$  and  $z = 2\lambda$ , i.e.  $\text{tr}(\widehat{W}_c(r, \varphi, r, \varphi, z))$ . In the second row, the profiles of the irradiance and the transversal  $\widehat{W}_c(r, \varphi, r, \varphi, z)_{11} + \widehat{W}_c(r, \varphi, r, \varphi, z)_{22}$  and longitudinal components  $\widehat{W}_c(r, \varphi, r, \varphi, z)_{zz}$  are presented. Note that for the beams we are handling, the magnitudes presented here only depend on  $r$  and  $z$ . As expected, the intensity of the transverse component is always zero at  $r = 0$ . In the next section a practical implementation of such kind of beams is explained.

#### 4. Experimental implementation

Figure 3 depicts an experimental setup based on a Mach-Zehnder interferometer able to generate arbitrary spatially-variant polarized focused beams. An extended explanation on how this system is used to generate beams with arbitrary polarization and shape can be found in [17]. An unpolarized quasi monochromatic input beam is split into two beams by means of polarizing beam splitter PBS<sub>1</sub>. Reflected by mirrors M<sub>1</sub> or M<sub>2</sub>, the split beam passes through wave plates HWP and QWP which rotate the oscillating plane and set the modulator to the required desired modulation curve. Then, light passes through a translucent SLM (Holoeye HEO 0017) displaying cell-based double-pixel holograms to encode complex transmittances  $E_{s_x}$  and  $E_{s_y}$  [38]. Using this holographic procedure, the displays can access nearly all possible complex values within a circle of transmittance  $T = 0.3$ , as explained in [18]. The beams are subsequently recombined by means of polarizing beam splitter PBS<sub>2</sub> and fed into a 4f system. A spatial filter removes higher-order terms whereas allowing pass the synthesized field. The irradiance of this beam can be observed by means of camera CCD<sub>1</sub>. Afterwards, the beam is focused by means of a high numerical aperture microscope lens NA=0.85. This objective obeys the sine condition thus  $P(\theta) = \sqrt{\cos \theta}$ . The field in the focal area is reflected on a glass surface and imaged on camera CCD<sub>2</sub>. Polarization analysis is carried out by means of polarizer LP and a quarter-wave plate.

In order to synthesize the beam of Eq. (24) the following complex valued distributions are coded on each SLM

$$E_{s_x} = i \sin \phi \cos \theta + \cos \phi \quad (26a)$$

$$E_{s_y} = -i \cos \phi \cos \theta + \sin \phi \quad (26b)$$

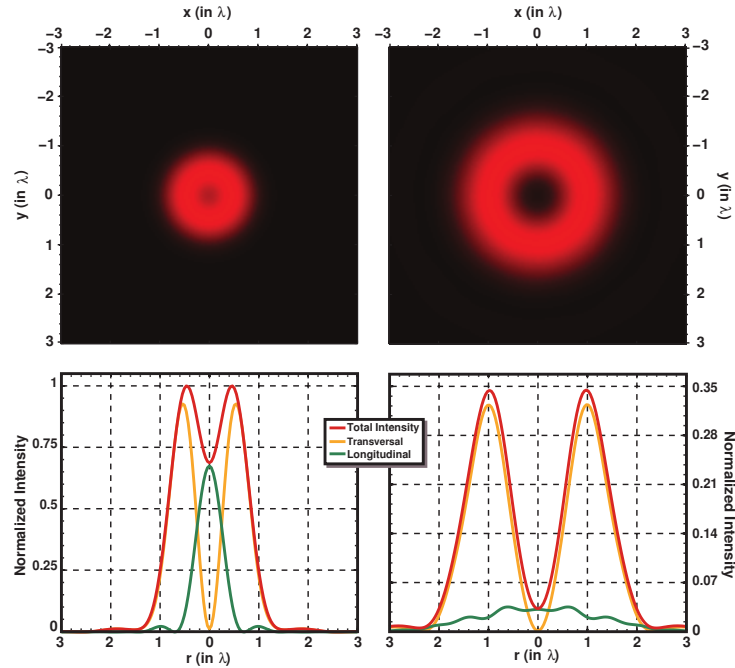


Fig. 2. Numerical simulation of Eq. (10) for the beam proposed in Eq. (24),  $NA=0.85$ . First row: false color representation of the intensity at  $z = 0$  and  $z = 2\lambda$ ; second row: profiles of the irradiance and the transversal and longitudinal components.

The observation plane (a cover slip) is mounted on a stage that enables to modify the observation distance  $z$ . Figure 4 shows the profile of  $C_0$  measured at  $z = 2\lambda$ . The distance of the observation plane with respect to the focal plane is estimated by comparing the experimental light distribution with the numerical evaluation of the angular average of the transversal irradiance. As shown in Fig. 4, the model developed reproduces with precision the profile of the transversal irradiance despite the fact that the value of this distribution at  $r = 0$  is not zero. The intensity detected at the center is compatible with certain amounts of background noise and spherical aberration of the imaging system. The focal plane cannot be retrieved with enough accuracy because of the insufficient resolution and limited bandwidth of the camera, and the lack of precision along the  $z$ -axis due to the equipment used.

Figure 5 summarizes the measures of the transversal Stokes parameters. The first row of Fig. 5 shows the parameters of the laser source measured in a plane between the optical fiber and lens  $L_1$ . The second and third rows display the Stokes parameters measured in two transverse planes in the focal area, in particular at  $z = 2\lambda$  and  $z = 4\lambda$ . In the three cases considered, parameters  $S_1$ ,  $S_2$  and  $S_3$  are close to zero at any point. Note that parameters  $C_0$ ,  $C_1$ ,  $C_2$  and  $C_3$  used in this paper are related to the conventional Stokes parameters by means of  $S_0=C_0$ ,  $S_1=C_2$ ,  $S_2=C_3$  and  $S_3=C_1$ . Table 1 indicates the averaged values of the Stokes parameters. For completeness, the averaged value of the degree of transversal polarization  $P_{2D}$  is also presented. Accordingly, the source beam is mostly unpolarized and the behavior of the Stokes parameters in the focal area is compatible with our thesis: the transverse component of the focused field remains unpolarized on axis.

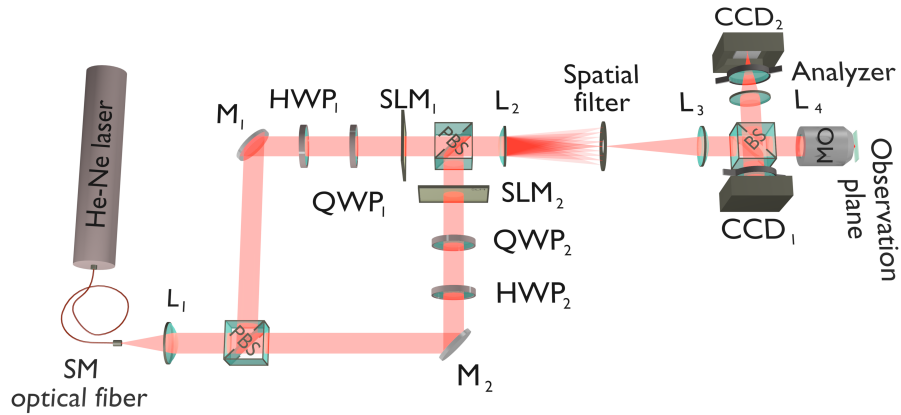


Fig. 3. Experimental setup

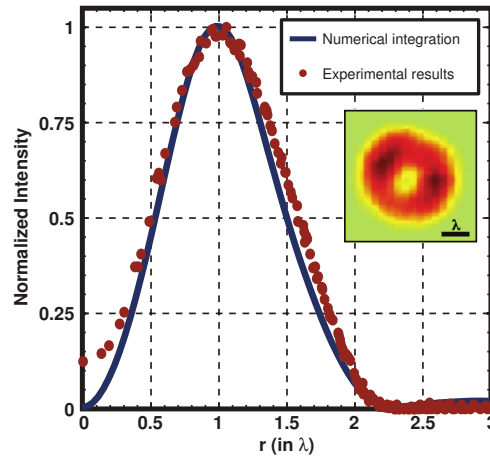


Fig. 4. Experimental  $C_0$  distribution at the focal area  $z = 2\lambda$ .

Table 1. Averaged normalized Stokes parameters.

	$S_1$	$S_2$	$S_3$	$P_{2D}$
He-Ne laser source	-0.06	0.04	0.04	0.10
$z = 2\lambda$	0.08	-0.02	0.01	0.08
$z = 4\lambda$	-0.04	0.03	-0.01	0.10

## 5. Concluding remarks

We developed a suitable framework for designing some transversal features of the field distribution in the focal region of a high numerical aperture lens when the incoming beam is partially polarized. In particular, we propose a field with a non-polarized transversal part that preserves this characteristic for any  $z$  and non-zero longitudinal component on axis. The combined use of an interferometric setup for generating beams with arbitrary polarization and digital holography techniques enables the generation of such field in practice. Numerical and experimental results

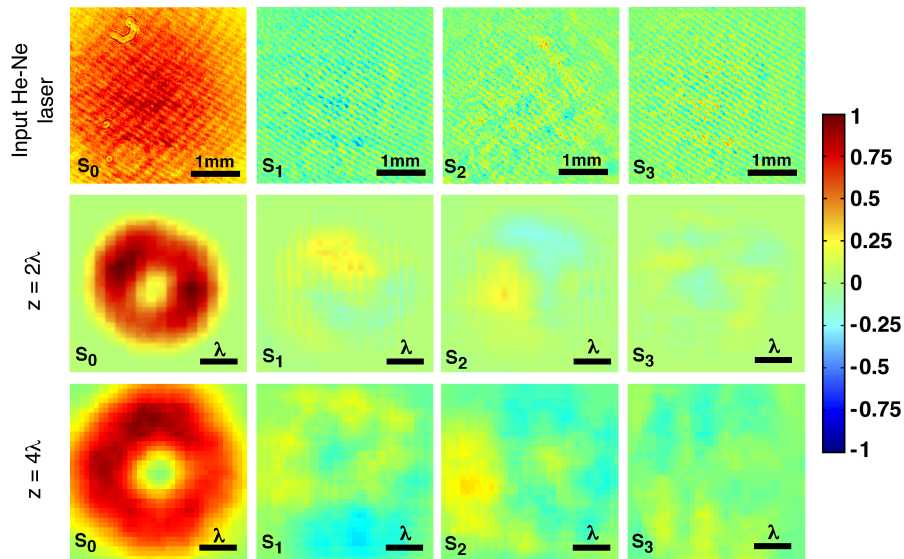


Fig. 5. Measure of the transversal Stokes parameters. First row: laser source; second and third rows: focal area of the microscope lens.

are provided, showing a good agreement between theoretical predictions and the experimental behavior of the beam.

### Acknowledgments

This work has been supported by the Ministerio de Ciencia e Innovación of Spain, project FIS2010-17543, and Ministerio de Economía y Competitividad projects FIS2013-46475.